Research Paper

GEOSPHERE

GEOSPHERE, v. 20, no. 3

https://doi.org/10.1130/GES02737.1

12 figures; 3 tables

CORRESPONDENCE: wuchen@itpcas.ac.cn

CITATION: Wu, C., Huang, K., Yin, A., Zhang, J., Zuza, A.V., Haproff, P.J., and Ding, L., 2024, Tectonic geomorphology and Quaternary slip history of the Fuyun fault, southwestern Altai Mountains, central Asia: Geosphere, v. 20, no. 3, p. 735–748, https://doi.org/10.1130/GES02737.1.

Science Editor: Andrea Hampel
Associate Editor: Xiaoming Shen

Received 22 November 2023
Revision received 21 February 2024
Accepted 11 March 2024

Published online 25 April 2024

Tectonic geomorphology and Quaternary slip history of the Fuyun fault, southwestern Altai Mountains, central Asia

Chen Wu[1,*], Ke Huang[2,*], An Yin[3,†], Jinyu Zhang[4], Andrew V. Zuza[5], Peter J. Haproff[6], and Lin Ding[1]

[1]State Key Laboratory of Tibetan Plateau Earth System and Resources Environment (TPESRE), Institute of Tibetan Plateau Research, Chinese Academy of Sciences, Beijing 100101, China
[2]Department of Mineral Geology, Guangdong Geological Bureau, Guangzhou 510080, China
[3]Department of Earth, Planetary, and Space Sciences, University of California, Los Angeles, California 90095, USA
[4]State Key Laboratory of Earthquake Dynamics, Institute of Geology, China Earthquake Administration, Beijing 100029, China
[5]Nevada Bureau of Mines and Geology, Nevada Geosciences, University of Nevada, Reno, Nevada 89557, USA
[6]Department of Earth and Ocean Sciences, University of North Carolina, Wilmington, North Carolina 28403, USA

ABSTRACT

The northwest-trending Altai Mountains of central Asia expose a complex network of thrust and strike-slip faults that are key features accommodating intracontinental crustal shortening related to the Cenozoic India-Asia collision. In this study, we investigated the Quaternary slip history of the Fuyun fault, a right-lateral strike-slip fault bounding the southwestern margin of the Altai Mountains, through geologic mapping, geomorphic surveying, and optically stimulated luminescence (OSL) geochronology. At the Kuoyibagaer site, the Fuyun fault displaces three generations of Pleistocene–Holocene fill-cut river terraces (i.e., T_3, T_2, and T_1) containing landslide and debris-flow deposits. The right-lateral offsets are magnified by erosion of terrace risers, suggesting that river course migration has been faster than slip along the Fuyun fault. The highest T_{p2} terrace was abandoned in the middle Pleistocene (150.4 ± 8.1 ka uppermost OSL age) and was displaced 145.5 +45.6/–12.1 m along the Fuyun fault, yielding a slip rate of 1.0 +0.4/–0.1 mm/yr since the middle Pleistocene. The lower T_{p1} terrace was abandoned in the late Pleistocene and aggraded by landslides and debris flows in the latest Pleistocene–Holocene (36.7 ± 1.6 ka uppermost OSL age). T_{p1} was displaced 67.5 +14.2/–6.1 m along the Fuyun fault, yielding a slip rate of 1.8 +0.5/–0.2 mm/yr since the late Pleistocene. Our preferred minimum slip rate of ~1 mm/yr suggests the Fuyun fault accommodates ~16% of the average geodetic velocity of ~6 mm/yr across the Altai Mountains. Integration of our new Fuyun slip rate with other published fault slip rates accounts for ~4.2 mm/yr of convergence across the Chinese Altai, or ~70% of the geodetic velocity field.

Chen Wu https://orcid.org/0000-0003-0647-3530
*Chen Wu (wuchen@itpcas.ac.cn), Ke Huang (huangke8807@163.com)
†Deceased

1. INTRODUCTION

Along-strike variations in slip rate and terminations of intracontinental strike-slip faults provide insight into their role in accommodating strain during orogeny. The central Asia and Tibetan Plateau regions serve as a natural laboratory for studying how intraplate strike-slip faults accommodate and redistribute strain related to various plate-boundary conditions, including the India-Asia collisional plate boundary to the south and the western Pacific subduction system plate boundary to the east. In particular, the major strike-slip faults distributed across central Asia are important structures in accommodating Cenozoic India-Asia convergence, including the Altyn Tagh, Kunlun, and Haiyuan faults in Tibet and the Fuyun and other strike-slip faults in the Altai Mountains (e.g., Cowgill, 2007; Cowgill et al., 2009; Frankel et al., 2010; Gold et al., 2011; Mériaux et al., 2005; Van der Woerd et al., 1998, 2002; Yin, 2010). The Fuyun active, right-lateral oblique thrust fault, located along the southern margin of the Altai Mountains, likely played a key role in constructing the Altai Mountains since the Oligocene (e.g., Calais et al., 2003; Yin, 2010; Klinger et al., 2011; Liang et al., 2021), yet its detailed slip history is not adequately constrained. Existing tectonic models for the Fuyun fault make different predictions for along-strike variations in Quaternary slip rates (e.g., Ding et al., 1985; Bai et al., 1996; Lin, 1994a, 1994b; Lin and Lin, 1998; Wang et al., 2001; Zhang et al., 2008a, 2008b; Klinger et al., 2011) that are not compatible with regional geodetic velocities (e.g., Calais et al., 2003, 2006; Yin et al., 1998; Gan et al., 2007; Yin, 2010; Fig. 1). Constraints on the Quaternary slip history of the Fuyun fault are also hindered by sparse age control in the region.

To address this issue and improve our understanding of the tectonic evolution of the Altai Mountains and central Asia, we conducted surficial geologic mapping, geodetic surveying, and luminescence geochronology along the Fuyun fault. We then compared our refined slip rate estimates for the Fuyun fault to regional geodetic velocities and slip rates for other strike-slip faults to improve our understanding of how active intracontinental deformation accommodates and partitions India-Asia convergence.

2. GEOLOGICAL SETTING

The Altai Mountains, located in central Asia between the Junggar Basin in the southwest and Great Lakes Valley in the northeast, expose a complex system of thrust and strike-slip faults that developed due to the Cenozoic India-Asia collision (Fig. 1; Cunningham, 1998, 2005; Cunningham

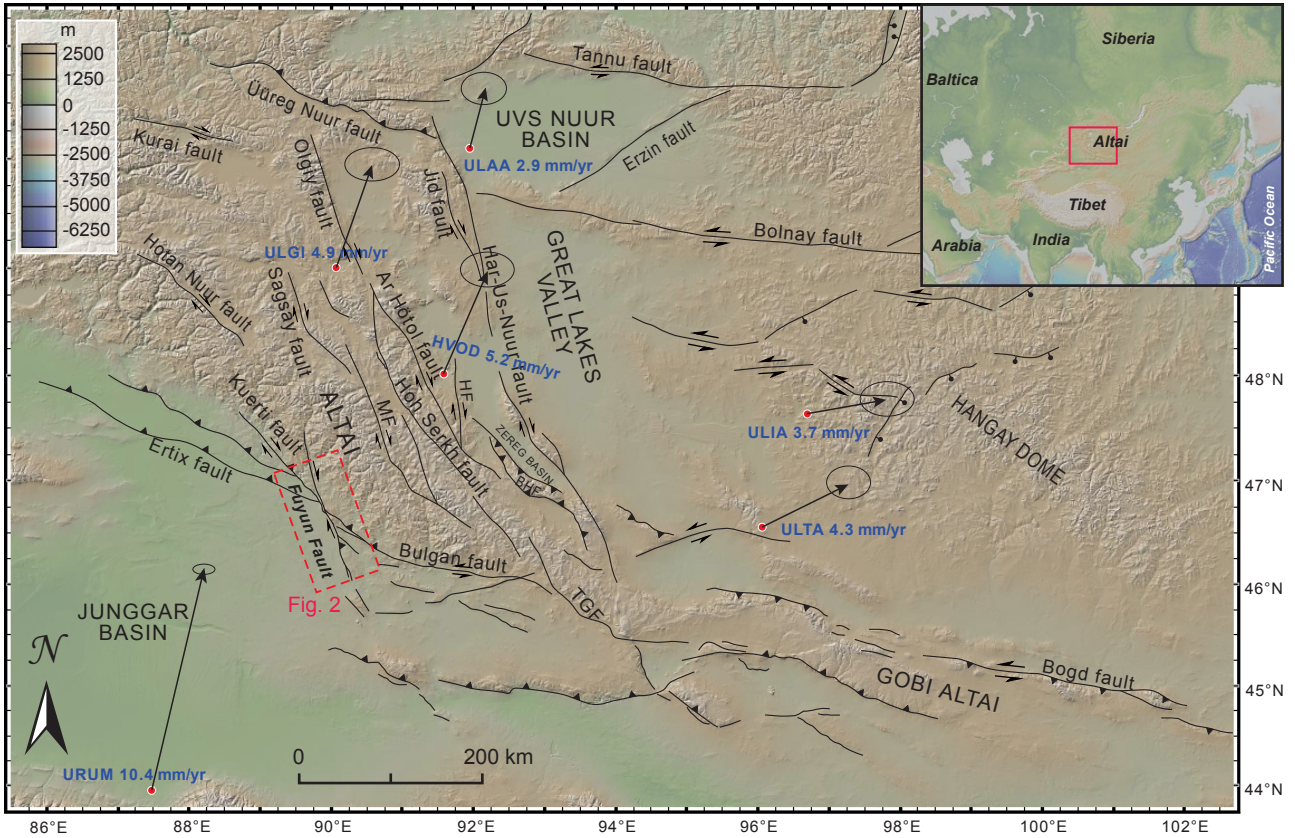

Figure 1. Map of active faults in the Altai Mountains region of central Asia from Tapponnier and Molnar (1979), Cunningham et al. (2003), Walker et al. (2006), Bayasgalan et al. (1999a, 1999b, 2005), Nissen et al. (2009), and Ritz et al. (1995). Red circles and black arrows denote the locations of global positioning system (GPS) stations and their velocities, respectively, based on Calais et al. (2003, 2006). The location of the study area is shown by the red dashed box. Base map is from Geomapapp.org (Ryan et al., 2009). HF—Hvod fault; MF—Mengildyk fault; TGF—Turgen Gol fault.

et al., 1996, 1997; Tapponnier and Molnar, 1979). Northeast-directed shortening across the Altai Mountains has been accommodated by northwest-striking thrust faults that are linked by strike-slip faults (Cunningham et al., 2003). These thrust and strike-slip faults from southwest to northeast consist of the Fuyun, Sagsay-Megildyk, Hoh Serkh, Ar Hötöl, Hovd, and Har-Us-Nuur faults (Cunningham et al., 2003; Cunningham, 2005, 2013). Several of these faults link with thrust and strike-slip faults in the Gobi Altai to the southeast (Cunningham et al., 2003; Cunningham, 2005, 2013; Fig. 1). The southwestern range front of the Altai Mountains is marked by the Fuyun fault (Fig. 1), an active, oblique right-lateral slip fault that initiated in the Oligocene (e.g., Klinger et al., 2011; Liang et al., 2021). Recent activity along the Fuyun fault was highlighted by a 1931 M_w ~8 earthquake near the Kalaxiangeer Mountain (Fig. 2; Ding et al., 1985).

Geodetic velocities throughout central Asia show that up to ~15% of the total India-Asia convergence is accommodated north of the Tian Shan (e.g., Yin et al., 1998; Gan et al., 2007; Yin, 2010). In this region, geodetic velocities decrease northward from ~10 mm/yr south of the Altai Mountains at Urumqi to ~4 mm/yr in the Altai Mountains and near zero on the Siberian platform (Fig. 1; Calais et al., 2003). About 6 mm/yr of India-Asia convergence is likely accommodated by right-lateral slip along north-northwest–striking faults in the Altai Mountains (Calais et al., 2003). Klinger et al. (2011) examined offset stream channels and terraces along the Fuyun fault and reported an average

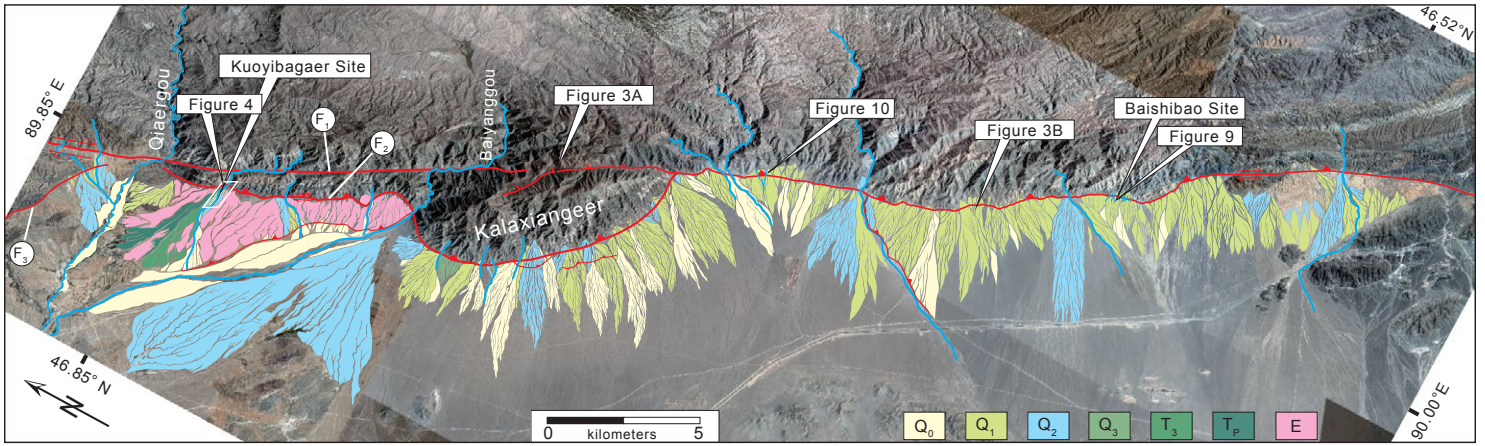

Figure 2. Quaternary surficial geologic map of the main segment of the right-lateral Fuyun fault. The eastern strand of the Fuyun fault (F_1) has a minor normal-slip component. The western strand of the Fuyun fault (F_2) has a reverse-slip component. "E" represents Paleocene–Eocene red inland lake strata; T_{p2} and T_3—Pleistocene alluvial terraces adjacent to Paleocene–Eocene red inland lake strata; Q_3, Q_2, Q_1, and Q_0—Quaternary alluvial fans composed of debris and sandy clay; F_3—Kuerti fault. Base map is from Google Earth.

right-lateral coseismic displacement of 6.3 m associated with the 1931 M_w ~8 earthquake. Results of microlite and pseudotachylite studies along the Fuyun fault suggest that the minerals formed during shallow seismic slip via selective melting under water-saturated conditions (Lin, 1994a, 1994b). Tree offsets and tree-ring analysis of *Sabina pseudosabina* specimens along the Fuyun fault zone indicate maximum surface displacements of ~10–15 m near the epicenter during the 1931 earthquake (Lin and Lin, 1998). Ding et al. (1985) examined offset geomorphic features along the Fuyun fault and reported right-lateral slip rates of 8.7 mm/yr since the middle Pleistocene, 19.5 mm/yr since the late Pleistocene, and 22.8 mm/yr during the Holocene. Based on offsets of stream channels, Bai et al. (1996) reported comparably slower right-lateral slip rates of 1.8 ± 0.1 mm/yr since the late Pleistocene and 3.8 ± 0.1 mm/yr during the Holocene. Zhang et al. (2008b) reported average Quaternary right-lateral slip rates for the Fuyun fault of 1.1–4.2 mm/yr based on offsets of stream channels. The results of these studies highlight how the slip rates along the Fuyun fault vary significantly based on the study site, time scales of displacement, and research group and methods.

3. METHODS

In this study, we performed neotectonic mapping of the Fuyun fault (Fig. 2) to identify and measure laterally offset Quaternary alluvial terraces. Key sedimentary horizons within offset terraces were dated via using luminescence geochronology to determine slip rates. Fault offsets of staggered terraces are usually measured as the distance between lines projected from each terrace edge to the fault trace (e.g., Cowgill, 2007; Cowgill et al., 2009). We examined offset alluvial fans along the Fuyun fault using 0.5-m-resolution Quickbird satellite imagery in Google Earth. Sites were mapped in the field, and remote sensing was used to differentiate different terrace surfaces and adjacent risers based on the relative heights of surfaces, inset relationships, and surface morphology and roughness (e.g., Cowgill, 2007; Cowgill et al., 2009). To measure offsets, we surveyed one site near Kuoyibagaer site using a Trimble 5700 real-time kinematic global positioning system unit, which has 10 mm horizontal and 20 mm vertical precision. AutoCAD software was used to measure offsets from the survey data. Surfer software was used to generate digital elevation models of sites along the Fuyun fault.

We performed optically stimulated luminescence (OSL) dating of sediment samples collected from terrace deposits at the Kuoyibagaer site (Table 1). OSL samples were collected by inserting steel tubes (5 cm diameter × 20 cm long) into sheltered terrace risers. Sedimentologic and stratigraphic details of the sample sites are described in the following sections. OSL sample tubes were wrapped with aluminum foil and tightened using plastic tape to prevent light and water contamination. OSL samples were processed and analyzed at the Institute of Hydrogeology and Environmental Geology, Chinese Academy of Geological Science, Shijiazhuang City, China. Prior to analysis, OSL samples were processed under subdued red light. Processing included pretreatment with 30% HCl and 40% H_2O_2 to remove carbonate and organic material, respectively, and immersion in H_2SiF_6 (30%) for 3 d to obtain quartz grains. Fine-grained quartz grains ~8–15 μm in diameter were isolated. All OSL analyses were performed under maximum power using a Daybreak2200 automated OSL reader equipped with blue (470 ± 5 nm, maximum power 60 mW/cm^2) and infrared (880 ± 80 nm, maximum power 80 mW/cm^2) light-emitting diodes and ^{90}Sr/^{90}Y beta sources (0.103871 Gy/s) for

TABLE 1. RESULTS OF OPTICALLY STIMULATED LUMINESCENCE (OSL) GEOCHRONOLOGY AT THE KUOYIBAGAER SITE

Sample no.		Depth (cm)	U (ppm)	Th (ppm)	K (%)	Equivalent dose (Gy)	Ambient dose rate (Gy/k.y.)	$Water_i/Water_e$ (%)	Age (ka)	Terrace tread
OSL-0a-1		15	2.21	8.93	2.44	15.95 ± 0.13	4.28	3.86	3.7 ± 0.2	Active channel
OSL-1a-1		10	2.38	13.7	2.34	19.74 ± 1.08	4.77	2.14	4.1 ± 0.3	T_0
OSL-1b	OSL-1b-1	15	2.19	8.81	2.36	13.57 ± 0.58	4.21	3.49	3.2 ± 0.2	
	OSL-1b-2	25	2.44	12.6	2.35	23.89 ± 1.18	4.58	5.62	5.2 ± 0.3	
	OSL-1b-3	40	2.35	10.1	2.21	23.53 ± 0.42	4.18	4.61	5.6 ± 0.2	
OSL-2a	OSL-2a-3	15	2.13	11.7	2.11	29.32 ± 1.26	4.22	3.37	6.9 ± 0.3	T_1
	OSL-2a-1	20	2.07	10.4	2.17	26.65 ± 1.05	4.06	6.07	6.6 ± 0.3	
	OSL-2a-2	30	2.16	11.5	2.00	61.44 ± 2.10	4.00	6.50	15.3 ± 0.8	
OSL-2b	OSL-2b-4	15	2.61	12.3	2.40	21.24 ± 1.25	4.66	5.56	4.5 ± 0.3	
	OSL-2b-3	30	2.62	13.1	2.28	21.17 ± 0.44	4.54	8.50	4.7 ± 0.2	
	OSL-2b-2	60	2.20	9.74	1.56	119.66 ± 2.22	3.26	14.93	36.7 ± 1.6	
	OSL-2b-1	80	2.25	11.4	1.69	138.30 ± 2.78	3.71	6.89	37.3 ± 1.7	
OSL-2d	OSL-2d-1	15	2.10	11.1	2.30	16.44 ± 0.56	4.32	3.98	3.8 ± 0.2	
	OSL-2d-2	25	2.24	13.7	2.24	46.55 ± 2.66	4.48	6.92	10.4 ± 0.7	
OSL-3a	OSL-3a-1	10	2.35	12.2	2.21	29.33 ± 0.40	4.42	4.08	6.6 ± 0.3	T_2
	OSL-3a-2	25	2.23	10.2	2.16	37.69 ± 2.92	4.08	6.22	9.2 ± 0.8	
	OSL-3a-3	30	2.19	9.80	2.45	49.72 ± 1.94	4.34	4.55	11.5 ± 0.6	
OSL-3b	OSL-3b-1	10	2.65	13.4	2.29	48.16 ± 1.52	4.59	8.90	10.5 ± 0.5	
	OSL-3b-2	15	2.19	9.56	1.93	100.21 ± 1.54	3.68	11.03	27.2 ± 1.2	
OSL-3c	OSL-3c-1	15	2.35	13.4	2.25	33.49 ± 1.42	4.53	6.13	7.4 ± 0.4	
	OSL-3c-2	30	2.25	11.5	1.96	40.85 ± 0.35	3.97	8.22	10.3 ± 0.4	
OSL-4a-1		25	2.29	10.3	2.10	68.30 ± 3.78	4.05	6.34	16.9 ± 1.2	T_3
OSL-4b-1		20	3.10	20.3	1.91	71.47 ± 3.37	5.14	5.16	13.9 ± 0.9	
OSL-5a-1		30	2.13	8.28	1.28	457.70 ± 16.40	3.04	3.29	150.4 ± 8.1	T_{p2}

irradiation. OSL samples were preheated prior to Li measurements (natural and regenerative OSL) at 260 °C for 10 s and prior to Ti measurements (test dose OSL) at 220 °C for 10 s. Equivalent doses for the OSL samples were obtained for fine-grained quartz grains following the sensitivity-corrected multiple-aliquot regeneration method. Neutron activation analysis was used to measure the U, Th, and K concentrations for all OSL samples.

4. RESULTS

4.1. Structure and Geomorphic Expression of the Fuyun Fault

The Fuyun fault is ~180 km long (47.5°N to 45.9°N latitude) and consists of several closely spaced, north-northeast–striking, right-lateral slip faults (Fig. 1). The eastern side of the Fuyun fault is the Altai Mountains foothills (~1800 m elevation; Fig. 2) composed of Devonian gneiss, phyllite, foliated tuff, and felsic stocks (Xinjiang BGMR, 1978). The western side of the Fuyun fault is a west-sloping alluvial plain (~1200 m elevation) composed of regional debris and sandy clay with pavement surfaces (Fig. 2). Scarps along the Fuyun fault occur within alluvial fans and have displaced stream drainages (Fig. 2; Ding, 1982). Strands along the northwestern Fuyun fault segment are discontinuous and have major extensional components as evidenced by mapped surface ruptures associated with the 1931 Fuyun earthquake (Ding et al., 1985). Normal slip along the northwestern Fuyun fault may have been responsible for opening the adjacent Keketuohai Lake and Tuerhong Basin (Fig. 1). Between Qiaergou to Kalaxiangeer, the central Fuyun fault splits into two strands, the northeastern and southwestern strands (Fig. 1). The southwestern fault strand (F_2 in Fig. 2) is a right-lateral thrust fault that forms a restraining bend at Kalaxiangeer Mountain (Fig. 1). F_2 continues southeastward along the southwestern margin of the Altai Mountains (Fig. 3B). The northeastern strand of the central Fuyun fault has displaced the Qiaergou and Baiyanggou river drainages and merges with the southwestern strand at the southeastern termination of the Kalaxiangeer restraining bend (Fig. 2). Younger normal faults evidenced by scarps have dissected the Kalaxiangeer restraining bend (Fig. 3A). The southeastern segment of the Fuyun fault is a discrete fault zone that splays into north-northwest–striking, en echelon thrust faults (Fig. 3B; Tapponnier and Molnar, 1979). These en echelon thrust faults have tilted Devonian strata on the eastern side of the fault and generated a depression on the western side of the fault (Fig. 3B).

4.2. Kuoyibagaer Site

At the Kuoyibagaer site, located north of the Kalaxiangeer restraining bend (46.82°N, 89.84°E), F_1

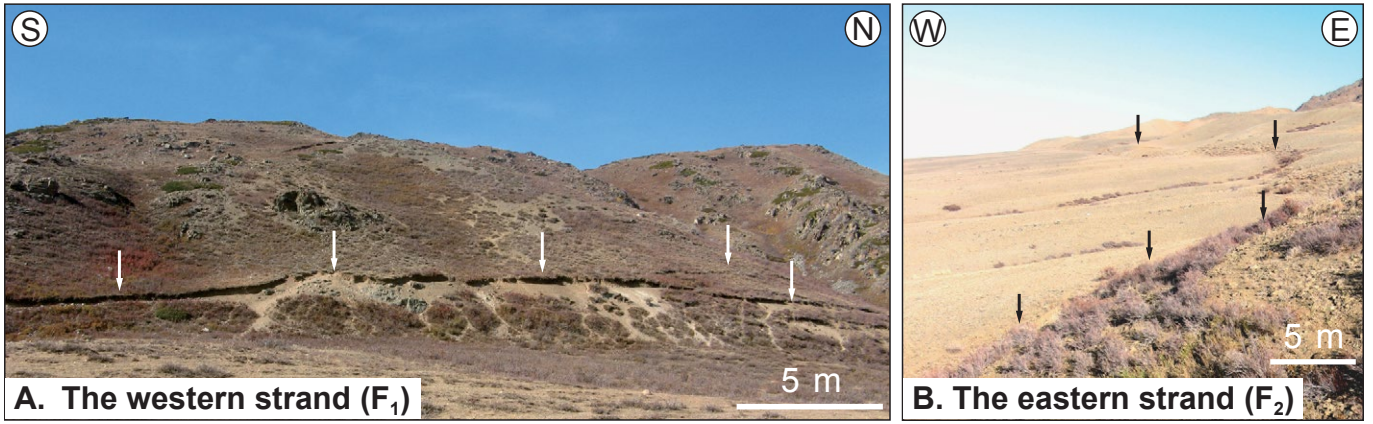

Figure 3. Field photographs of scarps along the Fuyun fault. (A) The western strand of the Fuyun fault has a normal-slip component north of Kalaxiangeer Mountain. (B) The eastern strand of the Fuyun fault has a reverse-slip component along the southern margin of the Altai Mountains.

and F_2 have displaced the west-flowing Kuoyibagaer river by ~1700 m (Fig. 2). Fluvial terraces associated with the Kuoyibagaer river are mostly located west of F_2 (Fig. 2). The eastern side of F_2 is a steep and narrow bedrock valley (Fig. 2). We interpreted F_2 is the most recently active surface trace of the Fuyun fault, whereas F_1 was interpreted as an older, potentially inactive fault strand. F_2 can be considered as the main fault. F_1 and F_2 may be linked at depth, with the speculated wedge-shaped feature sandwiched in the middle like a flower structure.

4.2.1. Fluvial Terrace Distribution and Offsets

West of F_2 at the Kuoyibagaer site, we differentiated five Quaternary fluvial terrace units (T_{p2}, T_3, T_2, T_1, and T_0) based on their elevations (Fig. 4). On the southern side of the Kuoyibagaer river, west of F_2, portions of T_2 and T_1 are heavily eroded. As a result, the T_2/T_0 and T_1/T_0 risers on the southern side are not preserved. On the northern side of Kuoyibagaer river, fluvial terraces are displaced north of the active drainage and have measured offsets of 67.5 +14.2/–6.1 m for the T_1/T_0 riser d_1, 121.4 +8/–10 m for T_2/T_1 riser d_2, 217.1 +17.4/–13.4 m for T_3/T_2 riser d_3, and 145.5 +45.5/–12.1 m for T_{p2}/T_1 riser d_{p2}. Our methods of measuring offsets and determining their uncertainties are illustrated on Figure 5.

4.2.2. Terrace Stratigraphy and Results of OSL Geochronology

On the western side of the Fuyun fault, the Kuoyibagaer river has incised Paleocene–Eocene red inland lake strata, labeled "E" (Fig. 2; Xinjiang BGMR, 1978). The inland lake deposits were not directly related to the activity of the Kuoyibagaer river. Middle Pleistocene alluvial strata were deposited atop the Paleocene–Eocene strata (Xinjiang BGMR, 1978) and subsequently incised, forming the T_{p2} terrace. T_{p2} has an elevation of ~9 m above the active drainage and is composed of poorly sorted, subrounded gravels and mostly well-sorted and layered fluvial sand-gravel deposits. Three minor terraces (i.e., T_3, T_2, T_1) were mapped in T_{p2}. T_3 is only exposed along the northern side of active drainage. T_2 and T_1 are exposed along both sides of the active drainage, with the southern T_1 being poorly preserved due to erosion (Fig. 4). Sedimentary horizons within these minor terraces are typically ~2–5 m thick and contain coarse and angular pebble gravels, sand, and silt (Fig. 6). T_0 is the active drainage and is expressed by abandoned bars and braided channels. Details of geomorphic characteristics are described in Table 2. The terrace profile is shown in Figures 7 and 8.

In this study, we performed OSL geochronological analysis on terrace deposits to determine the terrace abandonment ages. OSL samples were collected from fine-grained layers deposited in a low-energy environment. Sampling locations and details are shown in Figures 4 and 6. The results of the OSL geochronology are listed in Table 1. Samples OSL-2a-1, OSL-3a-2, OSL-4b-1, and OSL-5a-1 yielded OSL ages of 6.6 ± 0.3 ka, 9.2 ± 0.8 ka, 13.9 ± 0.9 ka, and 150.4 ± 8.1 ka, respectively. OSL ages are generally older with stratigraphic depth, with the exception of few samples, most of which overlap within error (Table 1). We interpret that these OSL ages represent upper bounds on the terrace abandonment ages of T_1, T_2, T_3, and T_{p2}, respectively, given the potential incomplete bleaching of sediments in alluvial fans and high-energy fluvial environments (Rhodes, 2011).

Samples OSL-2b-1 and OSL-2b-2 were collected at stratigraphic depths of 80 cm and 60 cm, respectively, below the tread of T_1. These samples yielded OSL ages of 37.3 ± 1.7 ka and 36.7 ± 1.6 ka,

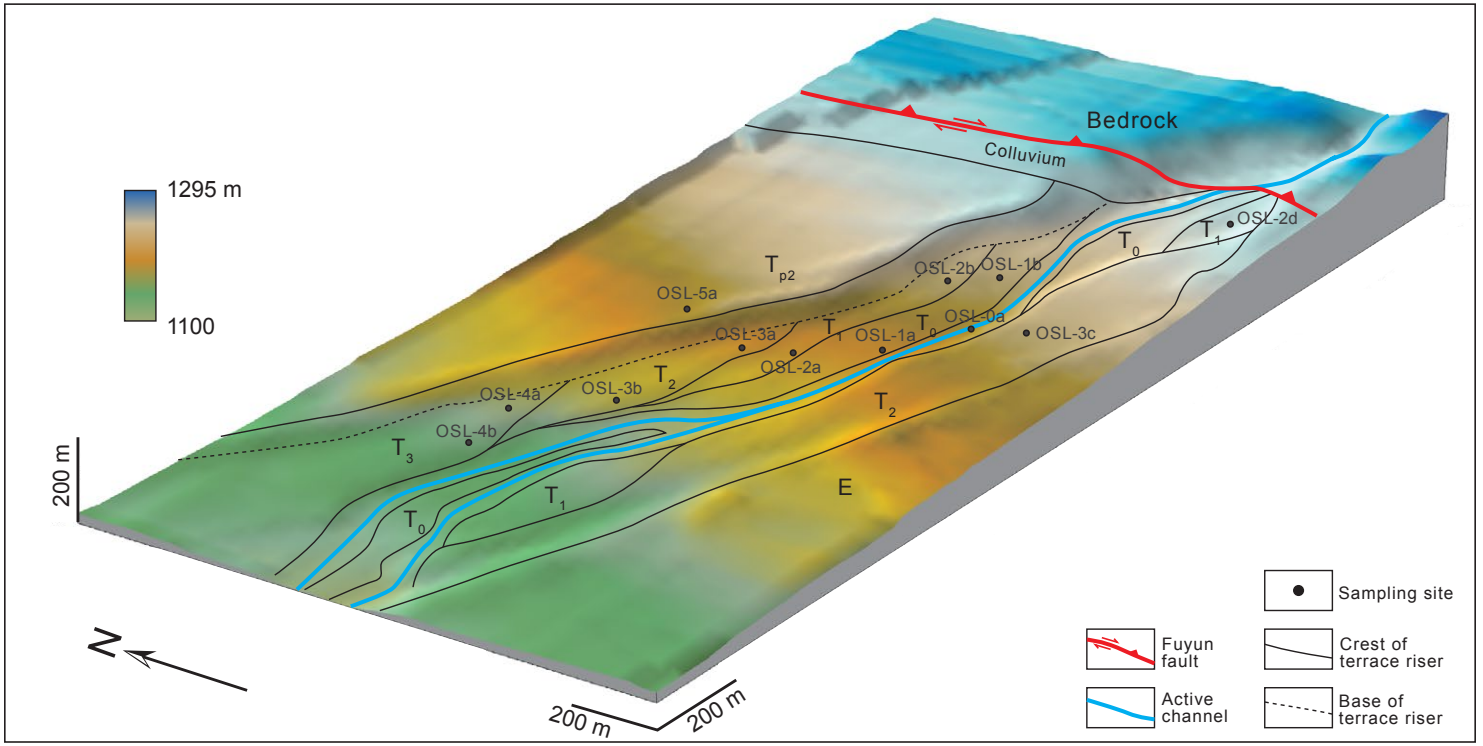

Figure 4. Three-dimensional digital elevation model showing the distribution of fluvial terraces at the Kuoyibagaer site along the Fuyun fault. T_{p2}, T_3, T_2, T_1, and T_0—Quaternary fluvial terrace units; E—Paleocene–Eocene red inland lake strata; OSL—optically stimulated luminescence.

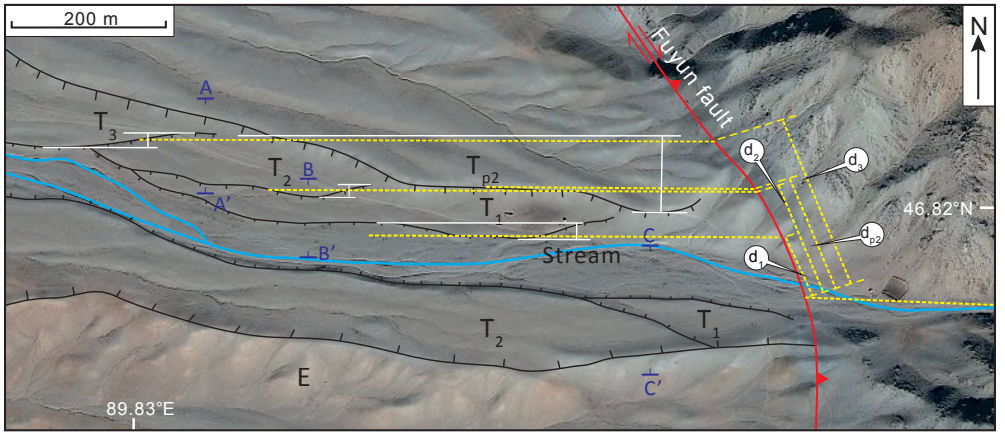

Figure 5. Map showing right-lateral offsets of fluvial terraces along the Fuyun fault at the Kuoyibagaer site. Offsets were measured in AutoCAD software based on the real-time kinematic surveying data. Separations are listed in Table 3. The trace of the Fuyun fault (red line) marks the contact between bedrock and Quaternary alluvium. Displacement measurements are shown as yellow lines. Uncertainties in displacement measurements are represented by white lines. The west-flowing, active stream channel is shown as light blue lines. Cross sections shown in Figure 8 are denoted by dark blue text and lines. Base map is from Google Earth.

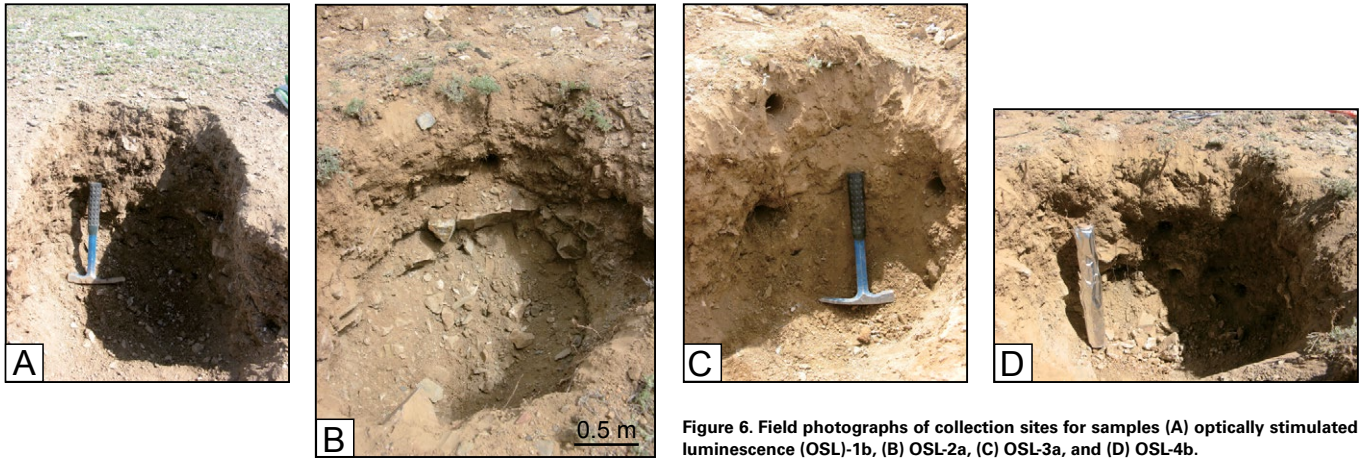

Figure 6. Field photographs of collection sites for samples (A) optically stimulated luminescence (OSL)-1b, (B) OSL-2a, (C) OSL-3a, and (D) OSL-4b.

TABLE 2. KEY GEOMORPHIC FEATURES AT THE KUOYIBAGAER SITE

Geomorphic surface	Height above active stream channel (m)	Topography	Soil-profile characteristics		Class of terrace	Samples
			Depth (cm)	Description		
T_0	0.5	Bar and braided channel	0–3	Thin and weak carbonate coating (Fig. 6A)	Active floodplain	
			3–50	Alluvial deposits with yellow-brownish sandy clay filling between poorly sorted subangular gravels (Fig. 6A)		OSL-1a-1,OSL-1b-1,OSL-1b-2,OSL-1b-3
T_1	2	Smooth tread with surface washing deposition	0–2	Gray-brownish active washing deposits and organic matter	Fill-cut terrace	
			2–30	Yellow-brownish sandy clay loam and coarse, angular gravel deposits (Fig. 6B)		OSL-2a-1, OSL-2a-3, OSL-2b-3, OSL-2b-4, OSL-2d-1
			30–80	Poorly sorted outwash deposits (Fig. 6B)		OSL-2a-2, OSL-2b-1, OSL-2b-2, OSL-2d-2
T_2	3.5	Smooth tread with surface washing deposition	0–2	Gray-brownish active washing deposits and organic matter	Fill-cut terrace	
			2–80	Yellow-brownish sandy clay loam and coarse, angular debris (Fig. 6C)		OSL-3a-1, OSL-3a-2, OSL-3a-3, OSL-3b-1, OSL-3b-2, OSL-3c-1, OSL-3c-2
T_3	5	Smooth tread with surface washing deposition and dendritic drainage incision in downstream reach	0–4	Gray-brownish active washing deposits and organic matter	Fill-cut terrace	
			4–50	Yellow-reddish sandy clay loam and angular gravel deposits (Fig. 6D)		OSL-4a-1, OSL-4b-1
T_{p2}	9	Ridge and ravine	0–4	Thin weathered material and organic matter	Fill terrace	
			4–70	Gray-yellow sandy clay loam and pebble gravels		OSL-5a-1
			70–140	Poorly sorted subrounded gravel deposits		
			150–350	Well-sorted and layered fluvial sand-gravel deposits		

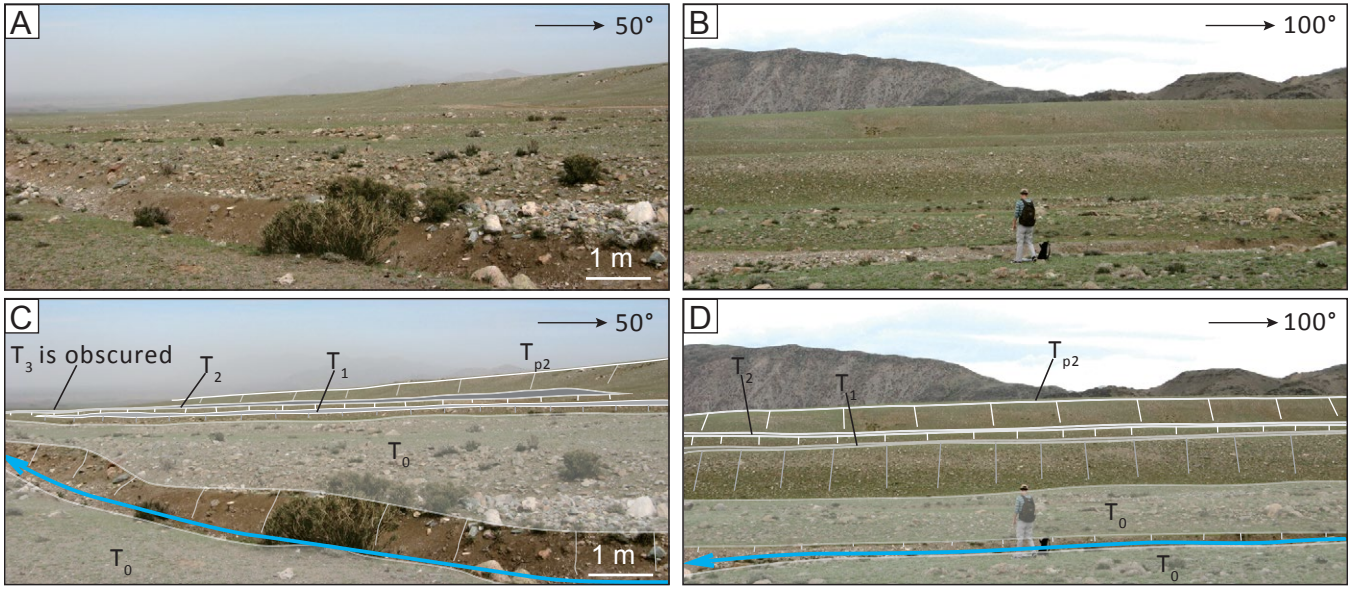

Figure 7. Field photographs of fluvial terraces and active channels at the (A–B) upstream and (C–D) downstream areas of the Kuoyibagaer river. The active stream channel is represented by light blue lines.

respectively. Whereas other samples collected in the uppermost part of T_1 yielded ages that clustered ca. 7–4 ka, these two samples are older than ages for samples from T_1, T_2, and T_3. For this reason, we assume that the beds from which samples OSL-2b-1 and OSL-2b-2 were collected are older than the sampled beds of T_1, T_2, and T_3.

4.3. Baishibao Site

Surficial ruptures of the central Fuyun fault are well expressed and laterally continuous (Fig. 2). The well-preserved piedmont surfaces along this fault segment contain numerous offset stream channels (Fig. 2). At the Baishibao site (46.58°N, 90.02°E), a surficial rupture cuts an alluvial fan and is associated with more than 10 right-lateral channel offsets along a 400 m section of the fault (Fig. 9). These right-lateral offsets are ~10 m as measured in Google Earth.

4.4. Saertuohai Site

At the Saertuohai site (46.09°N, 90.28°E), the southeastern Fuyun fault cuts two Quaternary fluvial terraces (T_{s2} and T_{s1}; Fig. 10C). T_{s2} is the highest and oldest terrace, and T_{s1} is the lower and younger terrace. The Fuyun fault has produced two offsets of T_{s2} and T_{s1} (d_{s2} and d_{s2}; Fig. 10D).

5. DISCUSSION

5.1. Terrace Chronology along the Fuyun Fault

In this study, we identified six levels of displaced fluvial terraces along the Fuyun fault (i.e., T_{p2}, T_{p1}, T_3, T_2, T_1, and T_0; Fig. 4). T_{p2} is a fill terrace that formed in the middle Pleistocene and was abandoned ca. 150 ka. From this finding, we interpret that the penultimate ice age of the Fuyun area terminated in the middle Pleistocene. T_{p1} is a fill terrace that is inset in T_{p2}, suggesting that the last ice age of the Fuyun area had ceased by the late Pleistocene. The youngest depositional age of T_{p1} inset in T_1 is ca. 37 ka. The upper layer of T_{p1} may have been eroded during the formation T_2 and T_1, and therefore its age does not represent the latest depositional timing of T_{p1}. However, the obtained age is the nearest abandonment age of T_{p1} in our samples. T_3, T_2, and T_1 are fill-cut terraces inset in T_{p1} that have abandonment ages of ca. 14 ka, ca. 9 ka, and ca. 7 ka, respectively, and they are interpreted to be related to younger episodic landslides and debris flows. T_0 is the active floodplain surface or an immature fill-cut terrace characterized by gravel bars.

5.2. Geomorphic Evolution at the Kuoyibagaer Site

Quaternary glaciations in the Altai Mountains consist of the Buerjin Ice Age in the middle

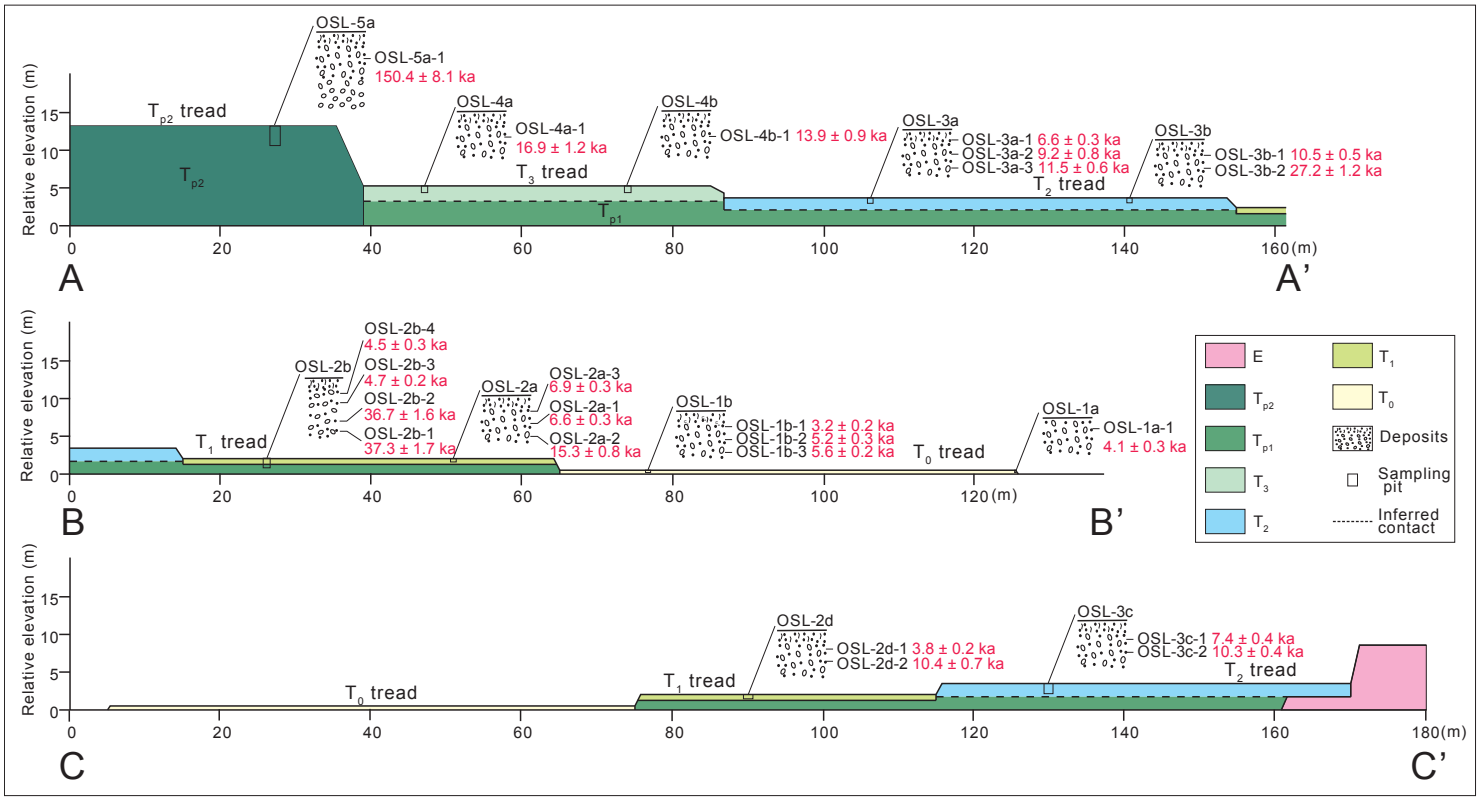

Figure 8. Cross sections depicting the sedimentology of fluvial terraces at the Kuoyibagaer site. See Figure 5 for cross-section locations. T_{p2}, T_{p1}, T_3, T_2, T_1, and T_0—Quaternary fluvial terrace units; E—Paleocene–Eocene red inland lake strata; OSL—optically stimulated luminescence.

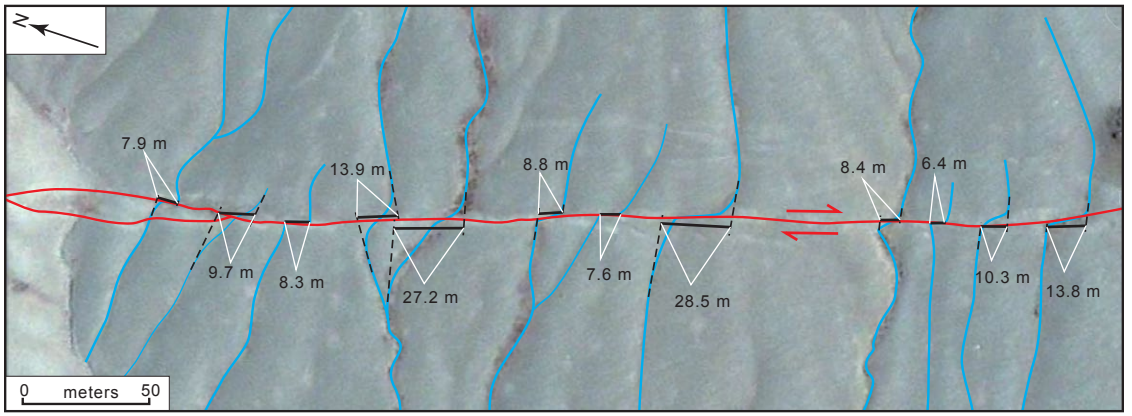

Figure 9. Map showing right-lateral offsets of stream channels along the Fuyun fault at the Baishibao site. The trace of the Fuyun fault is represented by the red line. Active stream channels are shown as light blue lines. Base map and offset measurements are from Google Earth.

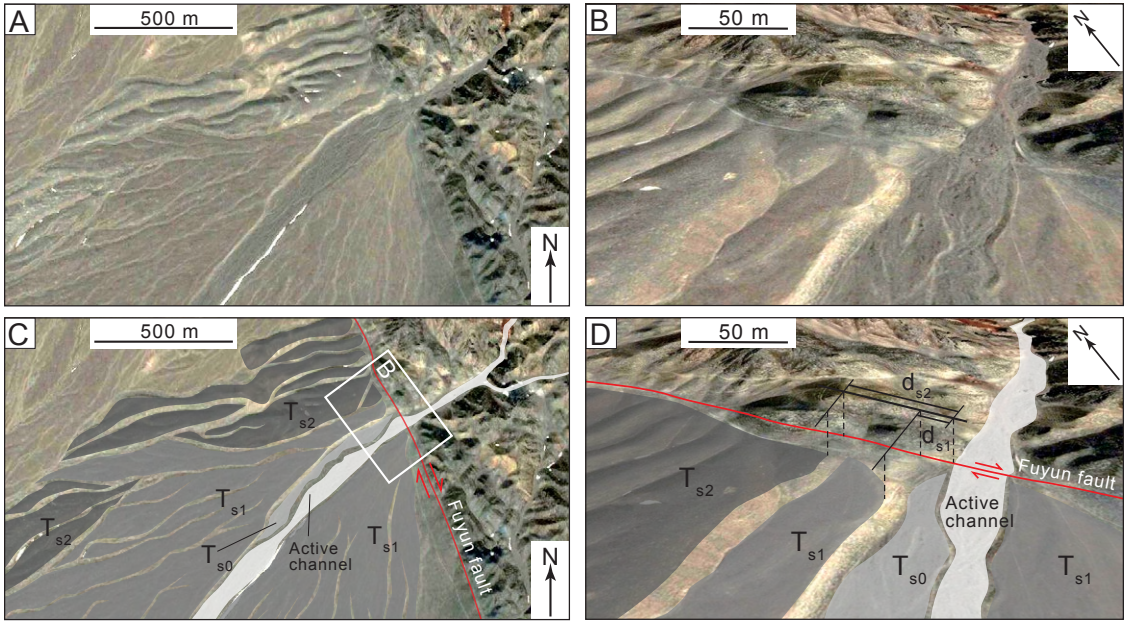

Figure 10. Maps of displaced fluvial terraces along the Fuyun fault at two locations (A/C and B/D) at the Saertuohai site. T_{s2}—oldest terrace, T_{s1}—younger terrace, T_{s0}—immature terrace; d_{s2} and d_{s1}—right-lateral offsets of the T_{s2}/T_{s1} riser and T_{s1}/T_{s0} riser, respectively. Base map is from Google Earth.

Pleistocene, the penultimate ice age at the end of the middle Pleistocene, the last ice age in the late Pleistocene, and the Neo-Ice Age neoglaciation and Little Ice Age in the Holocene (Zhao et al., 2013; Lehmkuhl and Owen, 2005). The ages of these glacial events determined via OSL dating of moraine deposits are ca. 476 ka for the Buerjin Ice Age, ca. 266–145 ka for the penultimate ice age, ca. 103 ka and ca. 32 ka for the last ice age, and ca. 4 ka for the Neo-Ice Age (Rudoy, 2002). As the climate warmed since ca. 10 ka, the Altai Mountains experienced a glacial retreat (Rudoy, 2002), which resulted in widespread alluviation in glacial valleys (Shi et al., 2006).

The Kuoyibagaer site is located at the outlet where piedmont discharge flows to the floodplain (Fig. 11). T_{p2} is a fill terrace that is inset in Paleocene–Eocene strata and contains at least 3.5 m of sediment. The space for this aggradation may have been induced by stream entrenchment during base-level fall as an ancient lake dried in the Junggar Basin since the late Eocene. Aggradation of a fill terrace requires large sediment yields and sufficient stream power to transport these sediments. Thus, we assume that T_{p2} was deposited during the transition between glacial and interglacial periods, while the warming climate melted glaciers and enhanced the stream power to transport weathered glacial sediments from the Altai Mountains to the Kuoyibagaer site. T_{p2} was described as middle Pleistocene alluvium in Xinjiang BGMR (1978). One OSL sample collected in this study from uppermost T_{p2} yielded an abandonment age of ca. 150 ka, which is slightly older than the youngest moraine age of the penultimate ice age in the Altai Mountains (Shi et al., 2006). This suggests that the penultimate ice age in the Fuyun area may have terminated during the middle Pleistocene.

At the Kuoyibagaer site, OSL results show that the depositional timing of the uppermost T_3, T_2, and T_1 clusters ca. 17–3 ka, whereas the lowermost T_1 depositional timing clusters ca. 37–27 ka. The ages of the uppermost, older terraces are younger than the lowermost, younger terraces, suggesting that the depositional timing of the uppermost T_2 and T_3 was more recent than that of the lowermost T_1. The uppermost, younger T_3, T_2, and T_1 thicknesses are less than 1 m. The coarse, angular deposits of these sedimentary horizons indicate their sediment was deposited in a high-energy environment. Thus, we consider that T_1, T_2, and T_3 at the outlet of Kuoyibagaer river experienced aggradation from landslides and debris flows, similar to the process described in Korup et al. (2004) and Selby (1988). Along the Fuyun fault, tectonic weakening made the gneiss and phyllite highly erodible and susceptible to slope failure. Warming climate conditions and glacial retreat during the Holocene may have provided the proper conditions for landslides and debris flows. The thin and coarse, uppermost T_3, T_2, and T_1 terraces were deposited as a result of landslides and debris flows during aggradation and subsequently abandoned during degradation. Under T_3, T_2, and T_1, one terrace was reformed by subsequent landslides, which we refer to as T_{p1}. Pleistocene deposits occur under T_1 but not T_0, suggesting that T_0 was the active drainage when T_{p1} was abandoned. This indicates that the T_{p1} riser is at least located under the T_1/T_0 riser.

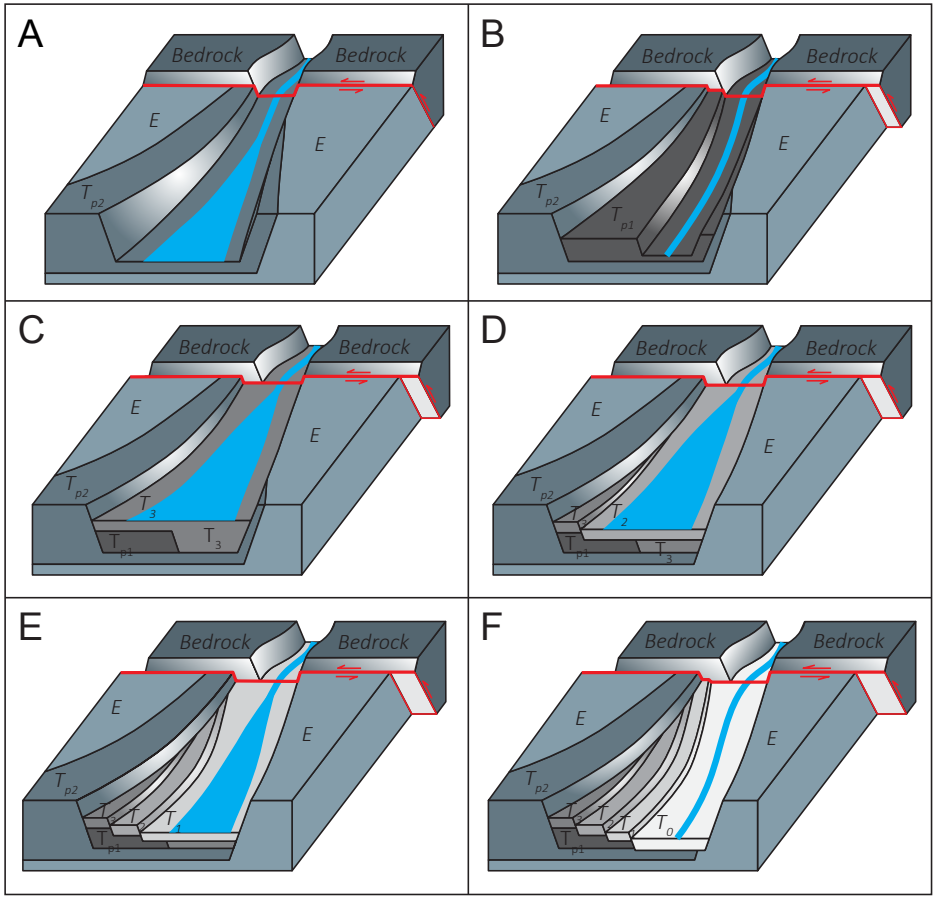

Figure 11. Model showing the geomorphic evolution and slip history of the Fuyun fault (F_2) at the Kuoyibagaer site. (A) T_{p2} was abandoned in the middle Pleistocene. (B) T_{p1} was abandoned in the late Pleistocene. (C) Landslides and debris flows induced aggradation of T_3 in the latest Pleistocene. (D) Landslides and debris flows induced aggradation of T_2 in the early Holocene. (E) Landslides and debris flows induced aggradation of T_1 in the middle Holocene. (F) T_1 was abandoned and T_0 was generated in the late Holocene. E—Paleocene–Eocene red inland lake strata.

From these findings, we interpret that the climatically induced aggradation of T_{p2} raised the active channel and provided the vertical space for degradation. An ~3 m thickness of T_{p2} was removed by stream downcutting during degradation (Fig. 11A). During the late Pleistocene, a climate-induced aggradational event, similar to the depositional event of T_{p2}, occurred in the Kuoyibagaer river, resulting in deposition of the fill terrace T_{p1} (Fig. 11B). The ages of samples OSL-2b-1 and OSL-2b-2 cluster ca. 37 ka, representing the depositional timing of T_{p1}, which coincides with the youngest moraine age of ca. 32 ka for the last ice age in the Altai Mountains. This overlap in ages suggests that aggradation of T_{p1} occurred during the late Pleistocene transition from the last ice age to an interglacial period.

As discussed above, T_3, T_2, and T_1 inset in T_{p1} were second-order responses to landslides and debris flows. Landslides and debris flows could provide rapid and high-energy sedimentation of T_{p1}, and the subsequent incision could down cut into T_{p1} and abandon the fresh tread. Thus, we consider that the T_3, T_2, and T_1 are fill-cut terraces that formed as the result of short-term, local adjustments of T_{p1} aggradation and landslides during the late Pleistocene–Holocene (Fig. 11).

The geomorphic evolution of the Kuoyibagaer site demonstrates the formation and reformation of fluvial terraces in a piedmont zone (Fig. 11). During a glacial period, the colder climate induced an increase in physical weathering and decrease in vegetation density in source regions such as mountains (e.g., Rudoy, 2002; Korup et al., 2004; Shi et al., 2006). Snow precipitation decreased stream power so that debris accumulated in the upstream area. Following the transition from a glacial to interglacial period, the warming climate produced abundant ice meltwater that enhanced stream power and transported debris to the downstream piedmont, resulting in terrace deposition. During the interglacial period, ice meltwater and sediment yields in the source region decreased. Although landslides and debris flows can induce rapid deposition on preexisting terraces, significant aggradation is rare, and degradation would be dominant in the river system (Fig. 11).

5.3. Slip Rates along the Fuyun Fault

Our constraints on the geomorphic evolution of the Kuoyibagaer site suggest that T_{p2} and T_{p1} are filled terraces that developed as long-term responses to climatic changes, whereas T_3, T_2, and T_1 are fill-cut terraces that developed as short-term responses to landslides and debris flows. The measured offset of the T_{p2} riser d_{p2} is 145.5 +45.5/–12.1 m (Figs. 5 and 12). The riser of T_{p1} is at least under the T_1/T_0 riser. From this, we assume the offset of T_{p1} riser d_{p1} is at least 67.5 +14.2/–6.1 m. The measured offsets of the T_3/T_2 riser d_3, T_2/T_1 riser d_2, and T_1/T_0 riser d_1 are 67.5 +14.2/–6.1 m, 121.4 +8/–9.9 m, and 217.1 +17.4/–13.4 m, respectively

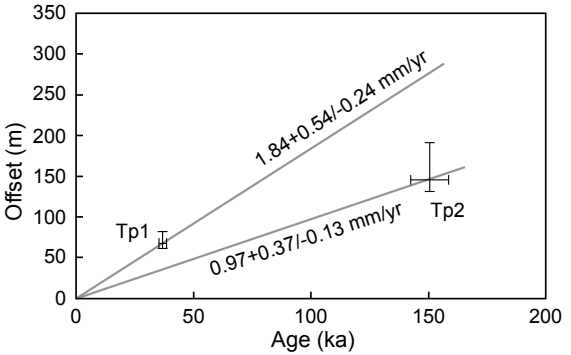

Figure 12. Plot of offset measurements (m) vs. luminescence age results (ka) showing slip rate estimates for the Fuyun fault at the Kuoyibagaer site. The lower-bound slip rate of 0.97 mm/yr since the middle Pleistocene corresponds to T_{p2}. The upper-bound slip rate of 1.84 mm/yr since the latest Pleistocene corresponds to T_{p1}. Table 3 shows the errors of slip rates.

(Table 3; Figs. 5 and 12). The measured offsets of the younger fill-cut terrace risers d_3, d_2, and d_1 are greater than those of the older fill terrace risers d_{p1} and d_{p2}. This suggests that river channel migration was faster than slip along the Fuyun fault since the latest Pleistocene, leading to overestimated offset measurements of the T_3/T_2 riser, T_2/T_1 riser, and T_1/T_0 riser. Faster river channel migration than fault slip has been identified along other faults, where it occurred, albeit on a much larger spatial scale and much longer temporal scale. In the southwestern Tibetan Plateau, the Indus River crossing the Karakorum fault migrated ~120 km (Gaudemer et al., 1989; Matte et al., 1996), whereas the fault offset is ~65 km (Murphy et al., 2000). In the northeastern Tibetan Plateau, the Huang He River crossing the Haiyuan fault migrated ~100 km (Gaudemer et al., 1989, 1995), whereas the fault offsets are ~10.5–15.5 km (Burchfiel et al., 1991). For the Kuoyibagaer site, we interpret that deflection of the river course by the Fuyun fault was followed by erosion of unconsolidated landslide and debris-flow deposits on the downstream cutbank of the river. This process gradually increased the apparent offset of the riverbank along the Fuyun fault and promoted river course migration.

Given the magnified right-lateral offsets of fill-cut terraces d_3, d_2, and d_1 due to erosion, we used the offsets of fill terraces T_{p2} and T_{p1} to estimate slip rates along the Fuyun fault. The offset of the T_{p2} riser (145.5 +45.5/–12.1 m) and its upper-terrace abandonment age of T_{p2} (150.4 ± 8.1 ka) yielded a minimum slip rate of 1.0 +0.4/–0.1 mm/yr since the middle Pleistocene (Table 3; Fig. 12). Because F_2 is a strand of the Fuyun fault, we suggest that the ~1 mm/yr rate is a minimum for the entire integrated Fuyun fault system. Our inferred offset of the T_{p1} riser (67.5 +14.2/–6.1 m) and its upper-terrace abandonment age of T_{p1} (36.7 ± 1.6 ka) yielded a slip rate of 1.8 +0.5/–0.2 mm/yr since the latest Pleistocene (Table 3; Fig. 12). Given the conservative offset estimate of the T_{p1} riser and potential that its OSL age is older than the actual abandonment age of T_{p1}, we assume that the ~1.8 mm/yr rate is slightly faster than the actual slip rate of the Fuyun fault.

TABLE 3. OFFSET MEASUREMENTS AND SLIP RATE ESTIMATES FOR THE KUOYIBAGAER SITE

Feature	T_{p2} riser	T_{p1} riser
Offset (m)	145.52 +45.46/–12.07	67.54 +14.24/–6.11
Sample	OSL-5a-1	OSL-2b-2
Upper-terrace abandonment age (ka)	150.4 ± 8.1	36.7 ± 1.6
Slip rate (mm/yr)	0.97 +0.37/–0.13	1.84 +0.54/–0.24

5.4. Comparison of Fuyun Fault Slip Rates and Geodetic Data

Calais et al. (2003, 2006) reported that ~15% of north-south India-Asia convergence is accommodated north of the Tien Shan based on geodetic velocities. These velocities decrease from south to north: from ~10.4 mm/yr north of the Tien Shan to ~2.9 mm/yr in the Uvs Nuur Basin (Fig. 1). Velocities of ~6 mm/yr and ~4.4 mm/yr are likely accommodated by north-northwest–striking right-lateral slip and thrust faults, respectively, in the Altai Mountains. Our minimum right-lateral slip rate of 1.0 +0.4/–0.1 mm/yr compared with the observed ~6 mm/yr average geodetic velocity across the Altai Mountains implies that at least ~17% of strike-slip motion across the Altai Mountains is accommodated by the Fuyun fault. Nissen et al. (2009) determined a maximum late Quaternary slip rate for the Har-Us-Nuur fault of 2.4 ± 0.4 mm/yr. Frankel et al. (2010) reported a minimum late Pleistocene slip rate of 0.8 +0.2/–0.1 mm/yr for the Hoh Serkh fault. Given our minimum right-lateral slip rate of 1.0 +0.4/–0.1 mm/yr since the middle Pleistocene, a total rate of ~4.2 mm/yr is accommodated along the integrated Fuyun, Har-Us-Nuur, and Hoh Serkh faults. In this sense, Quaternary slip rate studies for these faults can account for ~70% of the observed geodetic convergence rate across the Altai Mountains. The remaining slip may be accommodated by thrust faults or distributed off-fault deformation and complex rupture patterns (e.g., Pierce et al., 2021).

6. CONCLUSION

In this study, we performed geologic mapping, geomorphic surveying, and luminescence geochronological analysis of the Fuyun fault in the Chinese Altai to establish its Quaternary slip history. At the Kuoyibagaer site, climatic change–induced fill terraces T_{p2} and T_{p1} were formed in the middle Pleistocene at the end of the penultimate ice age and in the Pleistocene at the end of the last ice age, respectively. Fill-cut terraces T_3, T_2, and T_1 at the Kuoyibagaer site were formed in the latest Pleistocene–Holocene as short-term responses to

landslides and debris flows. Offsets of these fill-cut terraces along the Fuyun fault are magnified due to lateral erosion of unconsolidated terrace risers, indicating that river course migration was faster than slip along the fault. Measured offsets of Pleistocene terraces (145.5 +45.5/–12.1 m) and their interpreted abandonment age (150.4 ± 8.1 ka) yielded a minimum right-lateral slip rate of 1.0 +0.4/–0.1 mm/yr since the middle Pleistocene. Measured offsets of T_{p1} (67.5 +14.2/–6.1 m) and its interpreted abandonment age (36.7 ± 1.6 ka) yielded a minimum right-lateral slip rate of 1.8 +0.5/–0.2 mm/yr since the latest Pleistocene. Our minimum slip rate of ~1.0 +0.4/–0.1 mm/yr compared with the average geodetic velocity of ~6 mm/yr in the Altai Mountains suggests that at least ~16% of regional convergence is accommodated by right-lateral slip along the Fuyun fault zone. Integration of our new Fuyun slip rate with other published fault slip rates across the Altai Mountains accounts for ~70% of the average geodetic velocity field across the region.

ACKNOWLEDGMENTS

We thank Science Editor Andrea Hampel, Associate Editor Xiaoming Shen, Xiubin Lin, and an anonymous reviewer for their constructive comments that led to significant improvements in the original manuscript. This research was supported by grants from the National Natural Science Foundation of China (project no. 42372256), Basic Science Center for Tibetan Plateau Earth System (CTPES, 41988101), the Second Tibetan Plateau Scientific Expedition and Research Program (2019QZKK0708), and the Tectonics Program of the U.S. National Science Foundation (EAR-1914503, EAR-1914501, EAR-2210075, and EAR-2210074).

REFERENCES CITED

Bai, M., Luo, F., Yin, G., Xiang, Z., Shen, J., Shi, S., Ding, D., Guo, H., and Ruan, C., 1996, The Keketuohai-Ertai active fault zone: Inland Earthquake, v. 10, no. 4, p. 319–329.

Bayasgalan, A., Jackson, J., Ritz, J.F., and Carretier, S., 1999a, Field examples of strike-slip fault terminations in Mongolia and their tectonic significance: Tectonics, v. 18, no. 3, p. 394–411, https://doi.org/10.1029/1999TC900007.

Bayasgalan, A., Jackson, J., Ritz, J.F., and Carretier, S., 1999b, 'Forebergs', flower structures, and the development of large intra-continental strike-slip faults: The Gurvan Bogd fault system in Mongolia: Journal of Structural Geology, v. 21, no. 10, p. 1285–1302, https://doi.org/10.1016/S0191-8141(99)00064-4.

Bayasgalan, A., Jackson, J., and McKenzie, D., 2005, Lithosphere rheology and active tectonics in Mongolia: Relations between earthquake source parameters, gravity and GPS measurements: Geophysical Journal International, v. 163, no. 3, p. 1151–1179, https://doi.org/10.1111/j.1365-246X.2005.02764.x.

Burchfiel, B., Zhang, P., Wang, Y., Zhang, W., Song, F., Deng, Q., Molnar, P., and Royden, L., 1991, Geology of the Haiyuan fault zone, Ningxia-Hui Autonomous Region, China, and its relation to the evolution of the northeastern margin of the Tibetan Plateau: Tectonics, v. 10, no. 6, p. 1091–1110, https://doi.org/10.1029/90TC02685.

Calais, E., Vergnolle, M., San'kov, V., Lukhnev, A., Miroshnitchenko, A., Amarjargal, S., and Déverchère, J., 2003, GPS measurements of crustal deformation in the Baikal-Mongolia area (1994–2002): Implications for current kinematics of Asia: Journal of Geophysical Research: Solid Earth, v. 108, no. B10, 2501, https://doi.org/10.1029/2002JB002373.

Calais, E., Dong, L., Wang, M., Shen, Z., and Vergnolle, M., 2006, Continental deformation in Asia from a combined GPS solution: Geophysical Research Letters, v. 33, no. 24, L24319, https://doi.org/10.1029/2006GL028433.

Cowgill, E., 2007, Impact of riser reconstructions on estimation of secular variation in rates of strike-slip faulting: Revisiting the Cherchen River site along the Altyn Tagh fault, NW China: Earth and Planetary Science Letters, v. 254, no. 3–4, p. 239–255, https://doi.org/10.1016/j.epsl.2006.09.015.

Cowgill, E., Gold, R.D., Xuanhua, C., Xiao-Feng, W., Arrowsmith, J.R., and Southon, J., 2009, Low Quaternary slip rate reconciles geodetic and geologic rates along the Altyn Tagh fault, northwestern Tibet: Geology, v. 37, no. 7, p. 647–650, https://doi.org/10.1130/G25623A.1.

Cunningham, D., 2005, Active intracontinental transpressional mountain building in the Mongolian Altai: Defining a new class of orogen: Earth and Planetary Science Letters, v. 240, no. 2, p. 436–444, https://doi.org/10.1016/j.epsl.2005.09.013.

Cunningham, D., 2013, Mountain building processes in intracontinental oblique deformation belts: Lessons from the Gobi Corridor, central Asia: Journal of Structural Geology, v. 46, p. 255–282, https://doi.org/10.1016/j.jsg.2012.08.010.

Cunningham, D., Dijkstra, A., Howard, J., Quarles, A., and Badarch, G., 2003, Active intraplate strike-slip faulting and transpressional uplift in the Mongolian Altai, *in* Storti, F., Holdsworth, R.E., and Salvini, F., eds., Intraplate Strike-Slip Deformation Belts: Geological Society, London, Special Publication 210, p. 65–87, https://doi.org/10.1144/GSL.SP.2003.210.01.05.

Cunningham, W.D., 1998, Lithospheric controls on late Cenozoic construction of the Mongolian Altai: Tectonics, v. 17, no. 6, p. 891–902, https://doi.org/10.1029/1998TC900001.

Cunningham, W.D., Windley, B.F., Dorjnamjaa, D., Badamgarov, G., and Saandar, M., 1996, A structural transect across the Mongolian Western Altai: Active transpressional mountain building in central Asia: Tectonics, v. 15, no. 1, p. 142–156, https://doi.org/10.1029/95TC02354.

Cunningham, W.D., Windley, B.F., Owen, L.A., Barry, T., Dorjnamjaa, D., and Badamgarav, J., 1997, Geometry and style of partitioned deformation within a late Cenozoic transpressional zone in the eastern Gobi Altai Mountains, Mongolia: Tectonophysics, v. 277, no. 4, p. 285–306, https://doi.org/10.1016/S0040-1951(97)00034-6.

Ding, G., 1982, Offset streams and earthquakes in active strike-slip fault zone: Earthquake, v. 1, p. 3–8.

Ding, G., Shi, J., and Deng, Q., 1985, The Fuyun Active Fault Zone: Beijing, Seismological Press, 119 p.

Frankel, K.L., Wegmann, K.W., Bayasgalan, A., Carson, R.J., Bader, N.E., Adiya, T., Bolor, E., Durfey, C.C., Otgonkhuu, J., and Sprajcar, J., 2010, Late Pleistocene slip rate of the Höh Serh–Tsagaan Salaa fault system, Mongolian Altai, and intracontinental deformation in central Asia: Geophysical Journal International, v. 183, no. 3, p. 1134–1150, https://doi.org/10.1111/j.1365-246X.2010.04826.x.

Gan, W., Zhang, P.Z., Shen, Z. K., Niu, Z.J., Wang, M., Wan, Y.G., Zhou, D.M., and Cheng, J., 2007, Present-day crustal motion within the Tibetan Plateau inferred from GPS measurements: Journal of Geophysical Research: Solid Earth, v. 112, https://doi.org/10.1029/2005JB004120.

Gaudemer, Y., Tapponnier, P., and Turcotte, D., 1989, River offsets across active strike-slip faults: Annales Tectonicae, v. 3, no. 2, p. 55–76.

Gaudemer, Y., Tapponnier, P., Meyer, B., Peltzer, G., Shunmin, G., Zhitai, C., Huagung, D., and Cifuentes, I., 1995, Partitioning of crustal slip between linked, active faults in the eastern Qilian Shan, and evidence for a major seismic gap, the 'Tianzhu gap,' on the western Haiyuan fault, Gansu (China): Geophysical Journal International, v. 120, no. 3, p. 599–645, https://doi.org/10.1111/j.1365-246X.1995.tb01842.x.

Gold, R.D., Cowgill, E., Arrowsmith, J.R., Chen, X., Sharp, W.D., Cooper, K.M., and Wang, X.F., 2011, Faulted terrace risers place new constraints on the late Quaternary slip rate for the central Altyn Tagh fault, northwest Tibet: Geological Society of America Bulletin, v. 123, no. 5–6, p. 958–978, https://doi.org/10.1130/B30207.1.

Klinger, Y., Etchebes, M., Tapponnier, P., and Narteau, C., 2011, Characteristic slip for five great earthquakes along the Fuyun fault in China: Nature Geoscience, v. 4, no. 6, p. 389–392, https://doi.org/10.1038/ngeo1158.

Korup, O., McSaveney, M.J., and Davies, T.R.H., 2004, Sediment generation and delivery from large historic landslides in the Southern Alps, New Zealand: Geomorphology, v. 61, no. 1–2, p. 189–207, https://doi.org/10.1016/j.geomorph.2004.01.001.

Lehmkuhl, F., and Owen, L.A., 2005, Late Quaternary glaciation of Tibet and the bordering mountains: A review: Boreas, v. 34, no. 2, p. 87–100, https://doi.org/10.1080/03009480510012908.

Liang, Z., Wei, Z., Sun, W., and Zhuang, Q., 2021, Surface slip distribution and earthquake rupture model of the Fuyun fault, China, based on high-resolution topographic data: Lithosphere, v. 2021, https://doi.org/10.2113/2021/7913554.

Lin, A., 1994a, Glassy pseudotachylyte veins from the Fuyun fault zone, northwest China: Journal of Structural Geology, v. 16, no. 1, p. 71–83, https://doi.org/10.1016/0191-8141(94)90019-1.

Lin, A., 1994b, Microlite morphology and chemistry in pseudotachylite, from the Fuyun fault zone, China: The Journal of Geology, v. 102, p. 317–329, https://doi.org/10.1086/629674.

Lin, A., and Lin, S.-J., 1998, Tree damage and surface displacement: The 1931 M 8.0 Fuyun earthquake: The Journal of Geology, v. 106, no. 6, p. 751–758, https://doi.org/10.1086/516058.

Matte, P., Tapponnier, P., Arnaud, N., Bourjot, L., Avouac, J., Vidal, P., Qing, L., Yusheng, P., and Yi, W., 1996, Tectonics of western Tibet, between the Tarim and the Indus: Earth and Planetary Science Letters, v. 142, no. 3–4, p. 311–330, https://doi.org/10.1016/0012-821X(96)00086-6.

Mériaux, A.S., Tapponnier, P., Ryerson, F., Xiwei, X., King, G., Van der Woerd, J., Finkel, R., Haibing, L., Caffee, M., and Zhiqin, X., 2005, The Aksay segment of the northern Altyn Tagh fault: Tectonic geomorphology, landscape evolution, and Holocene slip rate: Journal of Geophysical Research: Solid Earth, v. 110, no. B4, B04404, https://doi.org/10.1029/2004JB003210.

Murphy, M., Yin, A., Kapp, P., Harrison, T., Lin, D., and Jinghui, G., 2000, Southward propagation of the Karakoram fault system, southwest Tibet: Timing and magnitude of slip: Geology, v. 28, no. 5, p. 451–454, https://doi.org/10.1130/0091-7613(2000)28<451:SPOTKF>2.0.CO;2.

Nissen, E., Walker, R.T., Bayasgalan, A., Carter, A., Fattahi, M., Molor, E., Schnabel, C., West, A.J., and Xu, S., 2009, The late Quaternary slip-rate of the Har-Us-Nuur fault (Mongolian Altai) from cosmogenic ^{10}Be and luminescence dating: Earth and Planetary Science Letters, v. 286, no. 3–4, p. 467–478, https://doi.org/10.1016/j.epsl.2009.06.048.

Pierce, I.K., Wesnousky, S.G., Owen, L.A., Bormann, J.M., Li, X., and Caffee, M., 2021, Accommodation of plate motion in an incipient strike-slip system: The central Walker Lane: Tectonics, v. 40, no. 2, https://doi.org/10.1029/2019TC005612.

Rhodes, E.J., 2011, Optically stimulated luminescence dating of sediments over the past 200,000 years: Annual Review of Earth and Planetary Sciences, v. 39, p. 461–488, https://doi.org/10.1146/annurev-earth-040610-133425.

Ritz, J., Brown, E., Bourles, D., Philip, H., Schlupp, A., Raisbeck, G., Yiou, F., and Enkhtuvshin, B., 1995, Slip rates along active faults estimated with cosmic-ray–exposure dates: Application to the Bogd fault, Gobi-Altaï, Mongolia: Geology, v. 23, no. 11, p. 1019–1022, https://doi.org/10.1130/0091-7613(1995)023<1019:SRAAFE>2.3.CO;2.

Rudoy, A.N., 2002, Glacier-dammed lakes and geological work of glacial superfloods in the late Pleistocene, southern Siberia, Altai Mountains: Quaternary International, v. 87, no. 1, p. 119–140, https://doi.org/10.1016/S1040-6182(01)00066-0.

Ryan, W.B., Carbotte, S.M., Coplan, J.O., O'Hara, S., Melkonian, A., Arko, R., Weissel, R.A., Ferrini, V., Goodwillie, A., Nitsche, F., Bonczkowski, J., and Zemsky, R., 2009, Global multi-resolution topography synthesis: Geochemistry, Geophysics, Geosystems, v. 10, Q03014, https://doi.org/10.1029/2008GC002332.

Selby, M.J., 1988, Landforms and denudation of the High Himalaya of Nepal: Results of continental collision: Zeitschrift für Geomorphologie Supplementband, v. 69, p. 133–152.

Shi, Y.F., Cui, Z.J., and Su, Z., 2006,Quaternary Glaciation and Environmental Variations in China: Shijiazhuang, China, Hebei Science and Technology Publishing House, 213 p.

Tapponnier, P., and Molnar, P., 1979, Active faulting and Cenozoic tectonics of the Tien Shan, Mongolia, and Baykal regions: Journal of Geophysical Research: Solid Earth, v. 84, no. B7, p. 3425–3459, https://doi.org/10.1029/JB084iB07p03425.

Van der Woerd, J., Ryerson, F.J., Tapponnier, P., Gaudemer, Y., Finkel, R., Mériaux, A.S., Caffee, M., Guoguang, Z., and Qunlu, H., 1998, Holocene left-slip rate determined by cosmogenic surface dating on the Xidatan segment of the Kunlun fault (Qinghai, China): Geology, v. 26, no. 8, p. 695–698, https://doi.org/10.1130/0091-7613(1998)026<0695:HLSRDB>2.3.CO;2.

Van der Woerd, J., Tapponnier, P., Ryerson, F.J., Meriaux, A.S., Meyer, B., Gaudemer, Y., Finkel, R.C., Caffee, M.W., Guoguang, Z., and Zhiqin, X., 2002, Uniform postglacial slip-rate along the central 600 km of the Kunlun fault (Tibet), from ^{26}Al, ^{10}Be, and ^{14}C dating of riser offsets, and climatic origin of the regional morphology: Geophysical Journal International, v. 148, no. 3, p. 356–388, https://doi.org/10.1046/j.1365-246x.2002.01556.x.

Walker, R., Bayasgalan, A., Carson, R., Hazlett, R., McCarthy, L., Mischler, J., Molor, E., Sarantsetseg, P., Smith, L., and Tsogtbadrakh, B., 2006, Geomorphology and structure of the Jid right-lateral strike-slip fault in the Mongolian Altay mountains: Journal of Structural Geology, v. 28, no. 9, p. 1607–1622, https://doi.org/10.1016/j.jsg.2006.04.007.

Wang, Q., Zhang, P.Z., Freymueller, J.T., Bilham, R., Larson, K.M., Lai, X., You, X., Niu, Z., Wu, J., and Li, Y., 2001, Present-day crustal deformation in China constrained by global positioning system measurements: Science, v. 294, no. 5542, p. 574–577, https://doi.org/10.1126/science.1063647.

Whitehouse, I.E., 1983, Distribution of large rock avalanche deposits in the central Southern Alps, New Zealand: New Zealand Journal of Geology and Geophysics, v. 26, no. 3, p. 271–279, https://doi.org/10.1080/00288306.1983.10422240.

Xinjiang Bureau of Geology and Mineral Resources (BGMR), 1978, Geologic Map of the Fuyun Area: Urumqi, Xinjiang, China, Xinjiang Bureau of Geology and Mineral Resources, scale 1:200,000.

Yin, A., 2010, Cenozoic tectonic evolution of Asia: A preliminary synthesis: Tectonophysics, v. 488, no. 1–4, p. 293–325, https://doi.org/10.1016/j.tecto.2009.06.002.

Yin, A., Nie, S., Craig, P., Harrison, T.M., Ryerson, F.J., Xianglin, Q., and Geng, Y., 1998, Late Cenozoic tectonic evolution of the southern Chinese Tian Shan: Tectonics, v. 17, no. 1, p. 1–27, https://doi.org/10.1029/97TC03140.

Zhang, P., Li, C., and Mao, F., 2008a, Strath terrace formation and strike-slip faulting: Seismology and Geology (Dizhen Dizhi), v. 30, no. 1, p. 44–57 [in Chinese].

Zhang, Z., Fu, B., and Awata, Y., 2008b, Late Quaternary systematic stream offsets along the Fuyun right-lateral strike-slip fault, Altay Mountains, China: Quaternary Sciences (Disiji Yanjiu), v. 28, no. 2, p. 273–279 [in Chinese].

Zhao, J., Yin, X., Harbor, J.M., Lai, Z., Liu, S., and Li, Z., 2013, Quaternary glacial chronology of the Kanas River Valley, Altai Mountains, China: Quaternary International, v. 311, p. 44–53, https://doi.org/10.1016/j.quaint.2013.07.047.